
Article:
Toso, L.F. orcid.org/0000-0001-8679-868X, Drummond, R. orcid.org/0000-0002-2586-1718 and Duncan, S.R. orcid.org/0000-0002-9525-7305 (2022) Regional stability analysis of transitional fluid flows. IEEE Control Systems Letters, 6. pp. 2287-2292. ISSN 2475-1456

https://doi.org/10.1109/lcsys.2022.3145233

Regional Stability Analysis of Transitional Fluid Flows

Leonardo F. Toso, Ross Drummond and Stephen R. Duncan

***Abstract*— A method to bound the maximum energy perturbation for which regional stability of transitional fluid flow models can be guaranteed is introduced. The proposed method exploits the fact that the fluid model's nonlinearities are both lossless and locally bounded and uses the axes lengths of the ellipsoids for the trajectory set containment as variables in the stability conditions. Compared to existing approaches based on quadratic constraints, the proposed method leads to an average increase in the maximum allowable energy perturbation of $\approx 29\%$ for the Waleffe-Kim-Hamilton (WKH) shear flow model and of $\approx 38\%$ for the 9-state reduced model of Couette flow.**

Index Terms— Fluid flows, regional stability analysis, semidefinite programming.

I. Introduction

Determining the stability properties of fluid flows remains a longstanding open problem tracing its roots back to Osborne Reynolds' 1883 experiments on the transition to turbulence in pipe flow [1]. The issues faced in predicting fluid stability are widely believed to be a result of the complex nature of the Navier-Stokes equations, which has forced practitioners to either solve these equations numerically using computational fluid dynamics (CFD) or adapt experimental results to predict a fluid's response. Both methods have their limitations; CFD simulations are computationally demanding and require expertise to run, while experimental results can be expensive and are also typically designed for demonstrative situations that may not generalise well to the flows found in practice. As a result, the design of many fluid-based technologies remains based upon significant experimental know-how and large computation power, an expensive and non-scalable situation.

The limitations of CFD simulations and experimental characterisations have led to the development of several reduced-order fluid models for particular flows, which have been shown to, at least qualitatively, give an indication of flow stability while being significantly simpler to resolve than the general Navier-Stokes equations. Examples include the 4-state Waleffe-Kim-Hamilton (WKH) model [2], [3] for shear flow and the 9-state reduced-order model [4] for Couette flow bounded by two plates. The apparent success of these reduced-order fluid models in capturing the main features of the flow has prompted research into their stability analysis, with the long term goal of this line of research being to generalise the lessons learned from these simpler systems to develop scalable and non-conservative techniques for the analysis of more complex fluid models.

Leonardo F. Toso, Ross Drummond and Stephen R. Duncan are with the Department of Engineering Science, University of Oxford, Oxford OX1 3PJ, United Kingdom. Email: {leonardo.toso, ross.drummond, stephen.duncan}@eng.ox.ac.uk.

The stability analysis of even these reduced-order models can still be challenging, owing to their nonlinear dynamics and non-normal state-transition matrices [5], [6]. However, progress has been made, notably in [7]–[9] where it was observed that the nonlinear model dynamics exhibit some structure that can be exploited. These studies observed that the model dynamics could be understood in terms of the feedback interconnection of a linear system with an energy persevering or lossless nonlinear gain, as shown in Figure 1, allowing the powerful and scalable techniques of passive systems theory [10, Chapter VI] to be applied. However, stability certificates based upon passive systems theory have been found to be conservative, and the maximum energy flow perturbation for which stability can be certified is significantly lower than that predicted by simulation (see Section VII). Reducing this conservatism will be necessary if these methods are to be deployed in practical applications involving more complex fluid flows.

Contribution: Motivated by the passive systems theory results [7]–[9], this paper extends the approach by introducing an algorithm that allows the axes lengths of the ellipsoids bounding the state trajectories to be defined as matrix variables to be optimised over. To evaluate the performance of the method, the obtained stability conditions were applied to both the 4-state WKH model for shear flow and the 9-state model of Couette flow and demonstrated a reduction in conservatism compared to [7]–[9] (see Section VII).

Paper structure: The paper is structured as follows. Section II introduces the two transitional fluid flow models, and Section III considers these models as the feedback interconnection of a linear system with a lossless nonlinearity, which allows passive systems theory to be applied to their analysis. Sections IV and V formulate bounds for the nonlinear flow interactions by exploiting the fact that the system's state trajectories can be bounded within an ellipsoidal region. By exploiting these local quadratic bounds, a method to certify the regional stability of these fluid models is developed in Section VI, with the main result presented in Theorem 1. Numerical results estimating the region of attraction of the Waleffe-Kim-Hamilton (WKH) model and the 9-state reduced-order model of Couette flow are described in Section VII to illustrate the potential of the approach.

Notation: The identity matrix of dimension n is I_n and the matrix of zeros of dimension $n \times m$ is $0_{n\times m}$. If a matrix A of dimension n is positive definite then $A \in \mathbb{S}^n_{\succ 0}$, if it symmetric then $A \in \mathbb{S}^n$ and if it is diagonal with positive elements then $A \in \mathbb{D}^n_{++}$. The ρ-level sets of a function $V(x)$ are defined as $\mathcal{E}(V,\rho) := \{x : V(x) = \rho\}$.

II. Transitional Fluid Flow Models

The transitional fluid flow models considered in this paper characterise the transition to turbulence in shear flows and are described by ordinary differential equations (ODEs).

A. General form

Both considered transitional fluid flows models can be expressed in the general form

$$\dot{x}(t) = Ax(t) + \phi(x) \tag{1}$$

where $x \in \mathbb{R}^n$ is the system's state, $A \in \mathbb{R}^{n\times n}$ is the Hurwitz state transition matrix depending on the Reynolds number (Re), and $\phi(x) = \mathcal{F}x \in \mathbb{R}^n \to \mathbb{R}^n$ describes the nonlinear interactions of the fluid flow. The nonlinearity $\phi(\cdot)$ can be expressed as a quadratic form $\phi^\top(x) = \left[x^\top S_1 x,\ \ldots,\ x^\top S_n x\right]$ with symmetric matrices $S_1, \ldots, S_n$.

B. Waleffe-Kim-Hamilton (WKH) shear flow model

The WKH model refers to the low-order fluid flow model formulated in [3] for characterising the transition to turbulence in shear flows. The model's equations were derived from observing direct numerical simulations (DNS) of Couette flow- a type of wall-bounded shear flow where the flow is driven by the relative motion of two plates, one moving and the other stationary. The model equations are

$$\begin{bmatrix}\dot{x}_1\\ \dot{x}_2\\ \dot{x}_3\\ \dot{x}_4\end{bmatrix} = \frac{1}{Re}\begin{bmatrix}-\lambda & 1 & 0 & 0\\ 0 & -\mu & 0 & 0\\ 0 & 0 & -\nu & 0\\ 0 & 0 & 0 & -\sigma\end{bmatrix}\begin{bmatrix}x_1\\ x_2\\ x_3\\ x_4\end{bmatrix} + \begin{bmatrix}x_2x_4 - \tau x_3^2\\ \delta x_3^2\\ \tau x_3(x_1 - \delta x_2)\\ -x_2x_1\end{bmatrix} \tag{2}$$

where x_1, x_2, x_3 and x_4 describe four modes of flow instability: streaks x_1, rolls x_2, inflectional streaks x_3 and mean shear x_4. The positive constants λ, μ, σ and ν concern the viscous decay rates, whereas τ and δ are positive nonlinear interaction coefficients.

A main feature of the WKH model is its ability to describe sustained turbulence [3]. This can be seen from simulations starting from the initial condition $[1, 0, 1, 0]^\top$. From this point, the model equations force the streaks to become increasingly inflectional, leading to a build-up in the rolls and energy being transferred between the various instability modes, prolonging the turbulence. See [3, Figure 6] for a more detailed description of this behaviour.

C. 9-state reduced model of Couette flow

The 9-state reduced-order model of Couette flow is a low-dimensional model generalised from the eight-mode model of [11] to capture variations in the main fluid velocity profile during the transition to turbulence. The nine ordinary differential equations of the model are detailed in [4] and are obtained by projecting the Navier-Stokes equations onto a set of finite-dimensional basis functions (specifically a set of nine normalised and orthogonal Galerkin modes [12]) over the spatial domain $0 \le b \le L_b$, $-1 \le c \le 1$ and $0 \le d \le L_d$. With b, c and d representing the downstream, shear and spanwise spatial directions, respectively. The nine modes of this model describe the mean velocity, streaks, instabilities of streaks, downstream vortices, and the nonlinear interaction between those variables. See [4, Figure 1] and [9, Figure 6] for further details on the model's configuration.

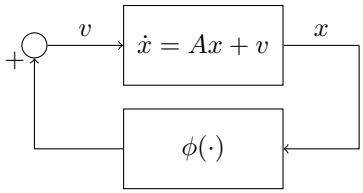

Fig. 1. *Feedback interpretation of* (1) *in terms of a linear system with a lossless nonlinearity.*

III. Feedback Interconnection of the Models

Accounting for the nonlinear terms $\phi(\cdot)$ in (1) is the main source of difficulty in the stability analysis of these models. However, for the transitional flow models considered here, these nonlinear terms exhibit properties that can be exploited. Specifically, well-established theory on the incompressible Navier-Stokes equations [13] (highlighted through the Leray formulation [14]) means that for many wall-bounded transitional fluid flow models, including [2] and [4], the nonlinearity $\phi(x)$ is *memoryless*, meaning that the mapping $\mathcal{F} : \mathbb{R}^n \to \mathbb{R}^n$ does not vary with time, satisfies $\phi(0) = 0$, and is *lossless*.

Definition 1: (Losslessness [10]) A nonlinear real function $\phi(x) = \mathcal{F}x$, with $\mathcal{F} : \mathbb{R}^n \to \mathbb{R}^n$, is said to be lossless if $x^\top\phi(x) = 0, \forall x \in \mathbb{R}^n$.

Losslessness of ϕ can also be encoded in a matrix form

$$\eta^\top \underbrace{\begin{bmatrix}0_{n\times n} & I_n\\ I_n & 0_{n\times n}\end{bmatrix}}_{F_0}\eta = 0, \quad \forall x \in \mathbb{R}^n, \tag{3}$$

with $\eta^\top = [x^\top,\ \ \phi^\top(x)]$, since $x^\top\phi(x) = \phi^\top(x)x = 0$.

By introducing the additional variable v, the model dynamics (1) can be equivalently written as

$$\dot{x} = Ax + v, \tag{4a}$$

$$v = \phi(x). \tag{4b}$$

As illustrated in Figure 1, this system can be understood as the feedback interconnection of a linear system with transfer function $(sI - A)^{-1}$ mapping $v \to x$ where v is the output from mapping the state x through the nonlinear, but lossless, gain $\phi(\cdot)$. The losslessness property of $\phi(\cdot)$ means that the feedback system's stability can be inferred using passive systems theory [10].

IV. Local quadratic bounds for ϕ

Globally, when considering $x \in \mathbb{R}^n$, losslessness is one of the only properties satisfied by $\phi(x)$; however, when considering a regional analysis with $x \in \mathcal{E} \subset \mathbb{R}^n$, the nonlinearity $\phi(x)$ can be locally bounded. The benefits of introducing local bounds for $\phi(\cdot)$ was identified in [7], with the bounds obtained from the Cauchy-Schwartz Lemma allowing the conservatism of their stability certificates to be reduced

compared to the earlier results of [8] and [9]. However, in general, bounds produced by the Cauchy-Schwartz Lemma are not tight, which suggests that there may be room to reduce this conservatism still further. Here, it is shown how by inspecting the various terms of the nonlinear term directly and bounding them, additional quadratic bounds for products of the nonlinear terms can be specified.

A. Local quadratic bounds

For the WKH model of (2), assume the states are bounded within the regions

$$ {x_1}^2 \leq \gamma_{x_1,k},\ {x_2}^2 \leq \gamma_{x_2,k},\ {x_3}^2 \leq \gamma_{x_3,k},\ {x_4}^2 \leq \gamma_{x_4,k} \quad (5) $$

for $k = 0, 1, \ldots, K$ with K being the total number of local quadratic bounds and define $\hat{\gamma}_{x_1,k} = \lambda_k \gamma_{x_1,k}$, $\hat{\gamma}_{x_2,k} = \lambda_k \gamma_{x_2,k}$, $\hat{\gamma}_{x_3,k} = \lambda_k \gamma_{x_3,k}$ and $\hat{\gamma}_{x_4,k} = \lambda_k \gamma_{x_4,k}$. With the states restricted as such, quadratic products of the nonlinear terms $\phi(.)$ can be bounded explicitly, as illustrated by the following example.

Example: Consider the cross-product between the nonlinearities $\phi_1(x)$ and $\phi_4(x)$ from (2),

$$ \begin{aligned} \phi_1(x)\phi_4(x) &= -{x_2}^2 x_4 x_1 + \tau {x_3}^2 x_2 x_1, && \text{(6a)} \\ &= \frac{{x_2}^2}{2}\left((x_4 - x_1)^2 - {x_4}^2 - {x_1}^2\right) && \text{(6b)} \\ &\quad + \frac{\tau {x_3}^2}{2}((x_2 + x_1)^2 - {x_2}^2 - {x_1}^2), \\ &\leq \frac{{x_2}^2}{2}(x_4 - x_1)^2 + \frac{\tau {x_3}^2}{2}(x_2 + x_1)^2. && \text{(6c)} \end{aligned} $$

Multiplying both sides of the above expression by λ_k and applying the state bounds (5) gives the local quadratic bound

$$ \begin{aligned} \lambda_k \phi_1(x)\phi_4(x) &\leq \frac{\tau\hat{\gamma}_{x_3,k}}{2}(x_2 + x_1)^2 + \frac{\hat{\gamma}_{x_2,k}}{2}(x_4 - x_1)^2, && \text{(7a)} \\ &= x^\top \underbrace{\begin{bmatrix} \frac{\tau\hat{\gamma}_{x_3,k}}{2} + \frac{\hat{\gamma}_{x_2,k}}{2} & \frac{\tau\hat{\gamma}_{x_3,k}}{2} & 0 & -\frac{\hat{\gamma}_{x_2,k}}{2} \\ \frac{\tau\hat{\gamma}_{x_3,k}}{2} & \frac{\tau\hat{\gamma}_{x_3,k}}{2} & 0 & 0 \\ 0 & 0 & 0 & 0 \\ -\frac{\hat{\gamma}_{x_2,k}}{2} & 0 & 0 & \frac{\hat{\gamma}_{x_2,k}}{2} \end{bmatrix}}_{\hat{\Gamma}_k(\hat{\gamma}_{x_2,k}, \hat{\gamma}_{x_3,k})} x. && \text{(7b)} \end{aligned} $$

By applying similar manipulations as (6), the WKH model's other nonlinear terms can also be bounded. For example

$$ \begin{aligned} \lambda_1 \phi_2(x)^2 &\leq \delta^2 {x_3}^2 \hat{\gamma}_{x_3,1}, && \text{(8a)} \\ \lambda_2 \phi_3(x)^2 &\leq \hat{\gamma}_{x_3,2}(\tau^2 {x_1}^2 + \tau\delta(x_1 - x_2)^2 + \delta^2 {x_2}^2), && \text{(8b)} \\ \lambda_3 \phi_4(x)^2 &\leq \hat{\gamma}_{x_2,3} {x_1}^2, && \text{(8c)} \\ \lambda_4 \phi_1(x)\phi_4(x) &\leq \frac{\tau\hat{\gamma}_{x_3,4}}{2}(x_2 + x_1)^2 + \frac{\hat{\gamma}_{x_2,4}}{2}(x_4 - x_1)^2, && \text{(8d)} \\ \lambda_5 \phi_3(x)\phi_4(x) &\leq \frac{\tau\hat{\gamma}_{x_1,5}}{2}(x_3 - x_2)^2 + \frac{\delta\hat{\gamma}_{x_2,5}}{2}(x_3 + x_1)^2, && \text{(8e)} \end{aligned} $$

with these inequalities parameterised by the state bounds of (5) and the nonlinear interaction coefficients τ and δ, and with the value of these coefficients influencing the tightness of the local quadratic bounds, and, consequently, the conservatism of the stability results.

Using a similar approach, additional bounds can be generated for the nonlinearities $\phi(\cdot)$ of the WKH and 9-state Couette flow models. The total number of bounds included in the analysis is defined as K, with a large K giving, in general, a tighter characterisation of the quadratic products of $\phi(.)$ but also an increase in computing time of the analysis, since it also increases the dimension of the search space for the Lagrange multiplier bounds, as explored in Algorithm 1. Moreover, the approach detailed in the above example can be automated, in some cases, to higher order polynomials than that considered in (6), for example via inequalities such as ${x_1}^4 \leq \gamma_{x_1,k} {x_1}^2$.

B. Matrix Inequalities

The local quadratic bounds of each models' nonlinearities can be expressed in a matrix form

$$ \eta^\top \underbrace{\begin{bmatrix} \hat{\Gamma}_k(\hat{\gamma}_{x_j,k}) & 0_{n\times n} \\ 0_{n\times n} & -\lambda_k M_k \end{bmatrix}}_{F_k(\hat{\Gamma}_k, \lambda_k)} \eta \geq 0,\ \forall x \in \mathcal{E}, \quad (9) $$

with M_k being a symmetric matrix corresponding to the k^{th} bound, with $k = 0, \ldots, K$ and the matrix $\hat{\Gamma}_k(\hat{\gamma}_{x_j,k}) \in \mathbb{S}^n$ being a symmetric matrix parameterised by the state bounds $\hat{\gamma}_{x_j,k}$. Equation (7b) details an example $\hat{\Gamma}_k(\hat{\gamma}_{x_j,k})$ matrix for a local quadratic bound. By incorporating these local bounds using the *S-procedure* [15], local information on $\phi(\cdot)$ can be included within the stability analysis, helping to reduce the conservatism.

As described in [7, Lemma 1], the nonlinearity $\phi(x)$ can also be bounded by

$$ \eta^\top \underbrace{\begin{bmatrix} S_i \Delta_i S_i & 0_{n\times n} \\ 0_{n\times n} & -\lambda_{K+i} e_i^T e_i \end{bmatrix}}_{M_i(\Delta_i, \lambda_{K+i})} \eta \geq 0, \forall x \in \mathcal{G}_\xi \quad (10) $$

for all $i = 1, \ldots, n$, with $\mathcal{G}_\xi = \{x \in \mathbb{R}^n : x(t)^\top G x(t) \leq \xi^2\}$ defining an ellipsoid over $\mathbb{R}^n$ and with $e_i \in \mathbb{R}^n$ being the i^{th} standard basis vector. Contrasting with the formulation of [7], in this paper, the matrices $\Delta_i = \lambda_{K+i}\xi^2 G^{-1}$ are defined as matrix decision variables in the optimisation problem of the stability conditions instead of being fixed at each iteration.

V. Ellipsoids for the set containment

For the local quadratic bounds on the nonlinear terms to hold, the state trajectories must be constrained to the local region $x \in \mathcal{E}$ for all initial conditions considered. The following proposition allows the ellipsoidal sets for this set containment to be posed in terms of linear matrix inequalities.

Proposition 1: Consider a Lyapunov function $V(x) : \mathbb{R}^n \to \mathbb{R}_+ = x(t)^\top P x(t)$ with $P \in \mathbb{S}^n_{\succ 0}$. For $k = 0, 1, 2, \ldots, K$, with K being the total number of bounds for $\phi(x)$ (Section IV), define ellipses $E_k(x) = x^T {\Lambda_k}^{-1} x = \sum_{j=1}^n {\gamma_{x_j,k}}^{-1} {x_j}^2$ where $\gamma_{x_j,k} > 0$, and the matrix $\hat{\Lambda}_k^{-1} = \frac{1}{\lambda_k}{\Lambda_k}^{-1}$. If

$$ \begin{bmatrix} P & \bar{\lambda}_k^{1/2} I_n \\ \bar{\lambda}_k^{1/2} I_n & \hat{\Lambda}_k \end{bmatrix} \succ 0, \quad \forall k = 0, 1, \ldots, K, \quad (11a) $$

$$ \bar{\lambda}_k \geq \lambda_k > 0, \quad \forall k = 0, 1, \ldots, K, \quad (11b) $$

then $\mathcal{E}(V,1) \subseteq \mathcal{E}(E_k,1)$ where $\mathcal{E}(V,1) := \{x \in \mathbb{R}^n : V(x) \leq 1\}$ and $\mathcal{E}(E_k,1) := \{x \in \mathbb{R}^n : x^\top {\Lambda_k}^{-1} x \leq 1\}$.

Proof: From the Schur complement, (11a) is equivalent to

$$P - (\bar{\lambda}_k)^{1/2} I_n (\hat{\Lambda}_k)^{-1} I_n (\bar{\lambda}_k)^{1/2} = P - \frac{\bar{\lambda}_k}{\lambda_k} {\Lambda_k}^{-1} \succ 0. \quad (12)$$

Since $\bar{\lambda}_k \geq \lambda_k > 0$, then (12) implies $P - {\Lambda_k}^{-1} \succ 0$. Multiplying this matrix inequality on the left by $x^\top$ and on the right by x gives $E_k(x) \leq V(x)$. We then have the set containment $\mathcal{E}(V,1) \subseteq \mathcal{E}(E_k,1)$. ■

VI. Regional stability of transitional flow models

Conditions to estimate the regional stability analysis can be formulated using the set containment of Proposition 1. In keeping with recent results, e.g., [7]–[9], these conditions enable inner estimates of the maximum energy perturbation guaranteeing asymptotic stability to be computed.

Theorem 1: Consider the system (1). For given $\epsilon > 0$ and $\bar{\lambda} \in \mathbb{R}^{n+K}_{\geq 0}$, if there exists positive-definite matrices $P \in \mathbb{S}^n_{\succ 0}$, $\hat{\Lambda}_k \in \mathbb{D}^n_{++}$, $\Delta_i \in \mathbb{S}^n_{\succ 0}$, $\hat{\Gamma}_k \in \mathbb{S}^n$ and Lagrange multipliers $\zeta_0 \in \mathbb{R}$, $\lambda_l \in \mathbb{R}^{n+K}_{\geq 0}$ that solves

$$\beta^* = \frac{1}{(R^*)^2} = \min_{P,\, \beta,\, \Delta,\, \hat{\Lambda}(\hat{\gamma}_{x_j,k}),\, \lambda,\, \zeta_0} \quad \beta = \frac{1}{R^2} \quad (13a)$$

subject to

$$\begin{bmatrix} A^\top P + PA & P \\ P & 0_{n\times n} \end{bmatrix} + \zeta_0 F_0 + \sum_{k=0}^{K} F_k(\hat{\Gamma}_k, \lambda_k) + \sum_{i=1}^{n} M_i(\Delta_i, \lambda_{K+i}) \preceq - \begin{bmatrix} \epsilon I_{n\times n} & 0_{n\times n} \\ 0_{n\times n} & 0_{n\times n} \end{bmatrix}, \quad (13b)$$

$$\begin{bmatrix} P & \bar{\lambda}_k^{1/2} I_n \\ \bar{\lambda}_k^{1/2} I_n & \hat{\Lambda}_k(\hat{\gamma}_{x_j,k}) \end{bmatrix} \succ 0, \quad \forall k = 0, \ldots, K, \quad (13c)$$

$$\begin{bmatrix} P & \bar{\lambda}_{K+i}^{1/2} I_n \\ \bar{\lambda}_{K+i}^{1/2} I_n & \Delta_i \end{bmatrix} \succ 0, \quad \forall i = 1, \ldots, n, \quad (13d)$$

$$0 \prec P \preceq \beta I_n, \quad (13e)$$

$$\bar{\lambda}_\ell \geq \lambda_\ell > 0, \quad \forall \ell = 1, \ldots, K+n, \quad (13f)$$

$$\hat{\Lambda}_k(\hat{\gamma}_{x_j,k}) \succeq 0, \quad \forall k = 0, \ldots, K, \quad (13g)$$

$$\Delta_i \succeq 0, \quad \forall i = 1, \ldots, n, \quad (13h)$$

then the system is asymptotically stable for all initial conditions $x(0) \in \mathcal{R} := \{x(0) \in \mathbb{R}^n : x(0)^\top x(0) \leq (R^*)^2\}$ with the trajectories satisfying the set containment $x \in \mathcal{R} \subseteq \mathcal{E}(V,1) \subseteq \mathcal{E}(E_k,1)$.

Proof: With the Lyapunov function $V(x(t)) = x(t)^\top P x(t)$, condition (13b) implies $\dot{V}(x(t)) < 0$ $\forall x \in \mathcal{E}(E_k,1)$. It is then required to show that the state trajectories remain within $\mathcal{E}(E_k,1)$ at all times. For this, it is noted that (13c) and (13f) imply via Proposition 1 that $\mathcal{E}(V,1) \subseteq \mathcal{E}(E_k,1)$. Similarly to the proof of Proposition 1, the constraints (13d) and (13f) imply that $\mathcal{E}(V,1) \subseteq \mathcal{G}_\xi$ if $V(x) \leq 1$. From (13e), then $0 \leq V(x) \leq \beta x(t)^\top x(t)$ when $x(0)^\top x(0) \leq R^2$, so $V(x(0)) \leq 1$. Condition (13b) means that the sublevel sets of $\mathcal{E}(V,1)$ are positive invariant, giving asymptotic stability. ■

Remark 1: Theorem 1 allows the axes lengths of the ellipsoids for the set containment (incorporated through the matrices $\hat{\Gamma}(\hat{\gamma}_{x_j,k})$ and $\hat{\Delta}$) to be decision variables in the problem. This formulation contrasts with [7, Algorithm A] where the ellipses are fixed at each iteration. However, to convexify the problem, the upper bound $\bar{\lambda}$ for the Lagrange multipliers λ have to be fixed when variable axes lengths are used. ⋆

Algorithm 1 Compute maximum energy perturbation R^*

1: **Set-up:** Obtain A, $\alpha^{\{m\}} = \epsilon_\alpha$, $\theta^{\{m\}} = \epsilon_\theta$ and tolerances ϵ, ϵ_β. Set $m = 0$
2: **Initialisation:** $\left(P^{\{0\}}, \lambda^{\{0\}}, \beta^{*\{0\}}\right) \leftarrow$ Solve Theorem 1 with (13f) replaced by (14)
3: $\bar{\lambda}^{\{0\}} = \frac{\lambda^{\{0\}}}{\beta^{*\{0\}}} \max\left(\text{eig}(P^{\{0\}})\right)$
4: **Define:** Directions $v^{\{j\}} \in \mathbb{R}^{n+K}$ for $j = 0, \ldots, n_v$
5: Set $\beta^{*\{0\}} = 0$ and $\bar{\omega}^{\{0\}} = \bar{\lambda}^{\{0\}}$
6: **while** $|\beta^{*\{m+1\}} - \beta^{*\{m\}}| \geq \epsilon_\beta$ **do**
7: **for** $j = 0, \ldots, n_v$ **do**
8: $\beta^{*\{m,j\}} \leftarrow$ Solve Theorem 1 with $\bar{\lambda} = \bar{\omega}^{\{j\}}$
9: **if** Theorem 1 is feasible **then**
10: $\bar{\omega}^{\{j\}} = \bar{\lambda}^{\{m\}} + \theta^{\{m\}} \beta^{*\{m\}} v^{\{j\}}$,
11: **else**
12: $\bar{\omega}^{\{j\}} = \bar{\lambda}^{\{m\}} + \theta^{\{m\}} \alpha^{\{m\}} v^{\{j\}}$,
13: **end if**
14: **end for**
15: Set $\beta^{*\{m+1\}} = \min_{j=0,\ldots,n_v} \beta^{*\{m,j\}}$
16: Set $\bar{\lambda}^{\{m+1\}} = \bar{\omega}^{\{j\}}$ that gives minimum $\beta^{*\{m,j\}}$
17: $m \leftarrow m + 1$
18: **end while**
19: $R^* = 1/\sqrt{\beta^{*\{m\}}}$

A. Convexification of Theorem 1

To pose Theorem 1 as convex optimisation, the upper bounds of the Lagrange multipliers $\bar{\lambda}$ have to be fixed. This restriction motivates the use of an iterative algorithm to refine the choice of $\bar{\lambda}$. In the following, an initialisation and update rule for $\bar{\lambda}$ is proposed, which is then embedded within Algorithm 1 to iteratively generate new bounds R^* and help reduce the conservatism of the approach.

Initialisation of $\bar{\lambda}$: One way to initialise $\bar{\lambda}^{\{m\}}$ in Algorithm 1 (with the notation $\{m\}$ indicating the value of the vector $\bar{\lambda}$ at iteration m) is to first solve Theorem 1 except with (13f) replaced by

$$\begin{bmatrix} \lambda_k & \bar{\lambda}_k^{1/2} \\ \bar{\lambda}_k^{1/2} & 1 \end{bmatrix} \succeq 0, \quad \forall k = 0, \ldots, K+n. \quad (14)$$

The above enforces $\lambda \geq \bar{\lambda} > 0$ instead of the upper bound of (13f). The reason for replacing (13f) with (14) in this modified version of Theorem 1 is because $\bar{\lambda}^{1/2}$ can then be defined as a matrix variable to be searched over in step 2 of the algorithm, giving flexibility. It is stressed though that this formulation of the problem can only be used to

initialise $\bar{\lambda}^{\{0\}}$, as it does not generate stability certificates as (13f) would not hold.

Update of $\bar{\lambda}$: Steps 10 and 12 in Algorithm 1 updates the upper bounds for the Lagrange multipliers to produce the iterates $\bar{\lambda}^{\{m\}}$. In these steps, candidate values for $\bar{\lambda}^{\{m\}}$ are proposed by stepping a distance $\theta \in \mathbb{R}$ in a direction $v^{\{j\}}$, which are both defined before the inner loop on j. In this work, the directions v were set to be (normalised) combinations of the basis vectors of dimension $n + K$ and their opposite directions, for instance $v^{\{1\}} = [0, 0, \ldots, 0]^\top, v^{\{2\}} = [1, 0, \ldots, 0]^\top, v^{\{3\}} = [0, 1, \ldots, 0]^\top, v^{\{4\}} = \frac{1}{\sqrt{2}}[-1, -1, \ldots, 0]^\top$ and so on for $j = 1 \ldots, n_v$, with the step lengths $\epsilon_\theta = 1$ and $\epsilon_\alpha = 10^4$. The algorithm then takes the value of $\bar{\lambda}^{\{m\}}$ which gave the biggest increase in $\beta^* = \frac{1}{R^2}$, and then continues onto the next iterate.

Remark 2: When the zero vector is included within the set of search directions v, step 16 ensure that Algorithm 1 is guaranteed to improve upon, or at least match, the obtained value of β^* computed upon each iteration m. ⋆

VII. Numerical Results

Numerical examples are now shown to evaluate the performance of Algorithm 1 in computing inner estimates of the region of attraction for the four and nine-state models. For both models, the maximal achievable energy perturbation obtained using Theorem 1 was compared against [9] and [7] as well as an upper limit produced by simulating the system from different initial conditions x_0's sampled from the hypersphere ${x_0}^\top x_0 = R^2$, with the upper limit obtained by finding the maximum value of R for which these simulated trajectories did not converge to the origin. For both examples, the parser CVX [16] was used along with the solver MOSEK [17] and tolerances $\epsilon = \epsilon_\beta = 10^{-6}$, $\epsilon_\alpha = 10^4$ and $\epsilon_\theta = 1$. The complete set of numerical results are detailed in Table I, with the // symbol used in this table indicating the result was not applicable.

A. Waleffe-Kim-Hamilton (WKH) shear flow model

Figure 2 shows the comparison for the WKH model described in Section II with the parameter values set to unity, as in $\sigma = \lambda = \ldots = \delta = 1$. While other parameter values have been used for this model, notably in [2], the choice of unity was selected to enable a direct comparison to the results of [7]. The maximal energy perturbation R^* was found for Reynolds numbers (Re) in the range $[5 : 5 : 25]$.

This figure shows the maximal energy perturbations allowed for both Algorithm 1 (green), [7], [9] (black), and the upper limit found through system's simulations (red). The results presented in Table I highlight how local quadratic bounds and the flexible computation of the ellipsoidal sets in Theorem 1 have significantly reduced the conservatism, meaning that a higher energy perturbation is allowed. Specifically, the average improvement over [7] for the five Reynolds numbers was $\approx 29\%$, while the average improvement over [9] for the five Reynolds numbers was $\approx 482\%$.

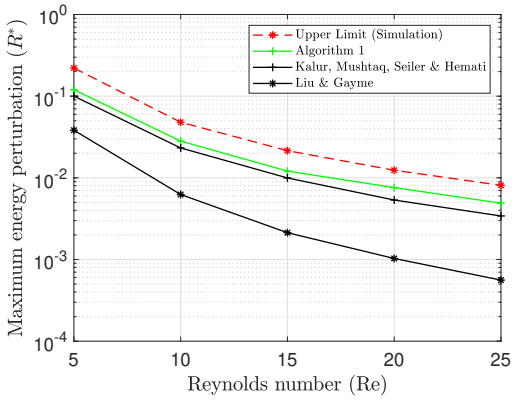

Fig. 2. *Comparison between [7], [9] and Algorithm 1 for bounding the maximum energy perturbations R^* of the WKH shear flow model.*

Two methods were introduced in this paper to reduce the conservatism of the stability conditions: the local quadratic bounds of Section IV and the computation of ellipsoids for the set containment of Section V. Table I allows the relative impact of these two methods to be compared, with the results for Algorithm 1 including the $K = 5$ bounds of the WKH model (8) but with results also shown for the case when $K = 0$, as in when no local quadratic bounds were included within the stability analysis. This table shows that including the local quadratic bounds only led to a modest increase in R^*, indicating that it was the computation of the ellipsoids for the set containment that delivered the more significant gains.

Figure 3 compares the convergence rate of Algorithm 1 without local quadratic bounds (K = 0) against [7, Algorithm A] for the WKH and 9-state model with different Reynolds numbers. In this case, the figure illustrates how Algorithm 1 required solving fewer optimisation problems to converge on its final value of R^*. As Table I shows, adding local quadratic bounds can increase the obtained value of R^*, but also increase the number of operations as more search directions have to be searched over.

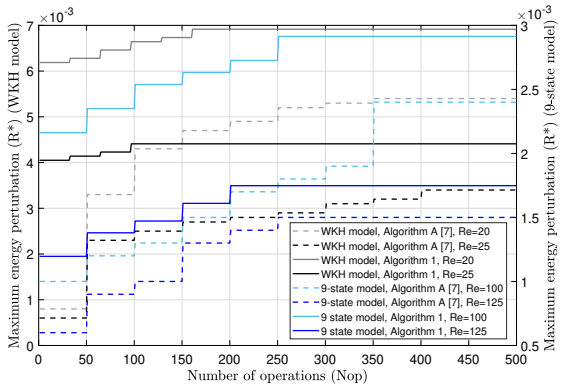

Fig. 3. *Convergence rates of Algorithm 1 with $K = 0$ and [7, Algorithm A] for bounding the maximum energy perturbations R^* of the WKH model (left-hand side axis) and 9-state model (right-hand side axis) with different Reynolds numbers. N_{op} corresponds to the number of optimisation problems solved during the algorithm run.*

	WKH model					9-state model				
Reynolds number (Re)	**5**	**10**	**15**	**20**	**25**	**100**	**125**	**150**	**175**	**200**
Methodology	**Maximum energy perturbation** (R^*)									
Upper limit (Simulation)	0.2210	0.0480	0.0215	0.0124	0.0081	//	//	//	//	//
Algorithm 1	0.1200	0.0282	0.0121	0.0076	0.0049	0.0031	0.0019	0.0013	0.0011	0.0009
Algorithm 1 without local quadratic bounds	0.1160	0.0266	0.0103	0.0069	0.0044	0.0028	0.0017	0.0012	0.0010	0.0008
Kalur, Mushtaq, Seiler & Hemati	0.1000	0.0232	0.0100	0.0054	0.0034	0.0024	0.0015	0.0010	0.0007	0.0006
Liu & Gayme	0.0383	0.0063	0.0021	0.0010	0.0006	0.0010	0.0006	0.0004	0.0003	0.0002

TABLE I

MAXIMUM ENERGY PERTURBATIONS R^* OF BOTH THE WKH AND THE 9-STATE COUETTE FLOW MODELS.

B. 9-state reduced-order model of Couette flow

A flow domain of $L_b = 1.75\pi$ and $L_d = 1.2\pi$ was defined for the numerical evaluation of the 9-state reduced-order model of Couette flow, with $K = 9$. Figure 4 compares the maximum achievable energy perturbation R^* for which stability could be verified, comparing Algorithm 1 (green) against [7] and [9] (black). Unlike for the WKH model, no upper limit for R^* could be found with this model at the considered Reynolds numbers using the method detailed at the start of this section; as in the simulated model's trajectories were observed to converge to the origin for all sampled initial conditions in the hyper-sphere ${x_0}^\top x_0 = R^2$ even for large R. The benefits of Theorem 1 were more striking for this model compared against the WKH model, with the improvement averaged across $\mathrm{Re} = [100 : 25 : 200]$ being $\approx 38\%$ over [7] and $\approx 253\%$ over [9].

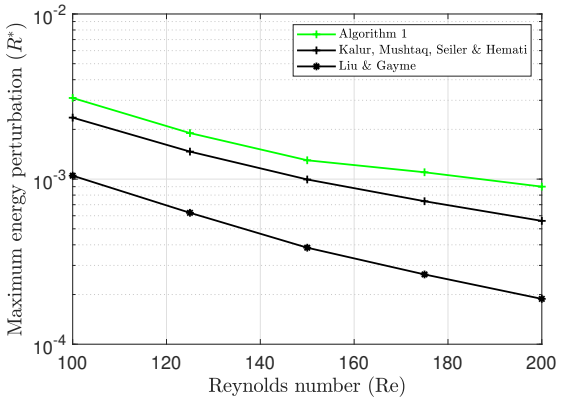

Fig. 4. *Comparison between [7], [9] and Algorithm 1 for bounding the maximum energy perturbations R^* of the 9-state Couette flow model.*

VIII. CONCLUSIONS

The regional stability analysis of transitional fluid flow models was considered. By exploiting the fact that the nonlinearities of these models are lossless and can be locally bounded, a method was proposed to determine the maximum energy perturbation in the flow field for which stability could be guaranteed. The potential of the proposed method was demonstrated through numerical examples which showed that the proposed method could reduce the conservatism in the stability guarantees compared against the current state-of-the-art for quadratic Lyapunov functions without sacrificing on computational efficiency. Future work will explore adapting the method for generic candidate Lyapunov functions and developing more effective ways to convexify the problem than the proposed method involving the $\bar{\lambda}$ bounds.

ACKNOWLEDGEMENTS

The authors gratefully acknowledge EDF Energy, UK, and the University of Oxford for supporting this research through a French internship scheme (sponsor license number UED4UGNF1). Ross Drummond was funded through a UKIC Fellowship from the Royal Academy of Engineering. The authors gratefully acknowledge the contributions from the anonymous reviewers, which greatly improved the paper.

REFERENCES

[1] O. Reynolds, "An experimental investigation of the circumstances which determine whether the motion of water in parallel channels shall be direct or sinuous and of the law of resistance in parallel channels," *Philos. Trans. R. Soc.*, vol. 82, 1883.

[2] F. Waleffe, "Transition in shear flows. nonlinear normality versus nonnormal linearity," *Physics of Fluids*, vol. 7, no. 12, p. 3060–3066, 1995.

[3] F. Waleffe, J. Kim, and J. M. Hamilton, "On the Origin of Streaks in Turbulent Shear Flows," *Turbulent Shear Flows 8*, pp. 37–49, 1993.

[4] J. Moehlis, H. Faisst, and B. Eckhardt, "A low-dimensional model for turbulent shear flows," *New Journal of Physics*, vol. 6, 05 2004.

[5] J. S. Baggett, T. A. Driscoll, and L. N. Trefethen, "A mostly linear model of transition to turbulence," *Physics of Fluids*, vol. 7, no. 4, pp. 833–838, 1995.

[6] L. N. Trefethen, A. E. Trefethen, S. C. Reddy, and T. A. Driscoll, "Hydrodynamic stability without eigenvalues," *Science*, vol. 261, no. 5121, pp. 578–584, 1993.

[7] A. Kalur, T. Mushtaq, P. Seiler, and M. S. Hemati, "Estimating Regions of Attraction for Transitional Flows Using Quadratic Constraints," *IEEE Control Systems Letters*, vol. 6, pp. 482–487, 2022.

[8] A. Kalur, P. Seiler, and M. S. Hemati, "Nonlinear stability analysis of transitional flows using quadratic constraints," *Phys. Rev. Fluids*, vol. 6, p. 044401, Apr 2021.

[9] C. Liu and D. F. Gayme, "Input-output inspired method for permissible perturbation amplitude of transitional wall-bounded shear flows," *Phys. Rev. E*, vol. 102, p. 063108, Dec 2020.

[10] H. K. Khalil, "Nonlinear systems," *3rd ed. Prentice-Hall*, 2002.

[11] F. Waleffe, "On a self-sustaining process in shear flows," *Physics of Fluids*, vol. 9, no. 4, pp. 883–900, 1997.

[12] P. Holmes, J. L. Lumley, and G. Berkooz, "Turbulence, Coherent Structures, Dynamical Systems and Symmetry," *Cambridge University Press*, 1996.

[13] P. J. Schmid and D. S. Henningson, "Stability and transition in shear flows," *Springer*, 2001.

[14] J. Leray, "Sur le mouvement d'un liquide visqueux emplissant l'espace," *Acta Mathematica*, vol. 63, 1934.

[15] C. A. Desoer and M. Vidyasagar, *Feedback systems: input-output properties*. SIAM, 2009.

[16] M. Grant and S. Boyd, "CVX: MATLAB Software for Disciplined Convex Programming, version 2.1," 2014.

[17] MOSEK ApS, *The MOSEK optimization toolbox for MATLAB manual. Version 9.0.*, 2019.